https://doi.org/10.2352/ISSN.2470-1173.2017.11.IMSE-180

Filter Selection for Multispectral Imaging Optimizing Spectral, Colorimetric and Image Quality

*Yixuan Wang, Roy S. Berns, Studio for Scientific Imaging and Archiving of Cultural Heritage, Program of Color Science, Rochester Institute of Technology, USA *Corresponding author: berns@cis.rit.edu*

Abstract

This paper will demonstrate the filter selection methods for wide band multispectral capturing system considering spectral and colorimetric reproduction as well as noise propagation. Spectral sensitivity of seven channel bandpass filter set was modeled and optimized first. Schott filters can be glued together to have bandpass shapes, which can be used to build the spectral camera. The glued Schott filters were selected based on the optimal modeling spectral sensitivity considering optical throughputs and infrared sensitivity. The second method to select the glued Schott filters is to divide the spectrum of interest evenly and select the combinations of filters whose peak wavelength were located in the range of spectrum subsets manually. An alternative option is to use single Schott filter set to build the spectral camera. However, although its spectral and colorimetric reproduction is accurate, single Schott filter set generates high propagated noise. Therefore, the glued Schott filters are preferred. The research provides insights for filter selection in multi-spectral camera design.

Introduction

Multi-spectral imaging and spectral reflectance reconstruction can be used in cultural-heritage institutes to digitalize their collections for documentation purposes. It can be used to simulate artwork under any lighting condition, and to analyze what type of colorants were used. The basic idea of a multi-spectral imaging system is to sub-sample spectral radiance, producing results similar to a spectrophotometer. The sampled data are used to reconstruct reflectance for the visible spectrum.

There are three basic schemes to build a multi-spectral imaging system: narrow bandpass filters with a monochrome imager, wide bandpass filters with a monochrome imager, and wide bandpass filters with a trichromatic digital camera (will be referred as dual-RGB as an abbreviation).

However, narrow band capture is not practical for cultural-heritage studio imaging because of its consuming measurements, complex image registration, geometric distortion and high cost of customized filters [1-4]. Dual-RGB utilizes two absorption filters with a trichromatic digital camera. Currently, the only commercial system that uses the dual-RGB technique with the utilization of professional medium format cameras is the Sinar CTM camera. This scheme is convenient since only two captures are needed to give the information of five channels (the spectral sensitivities of the two green channels with two different filters are close, so only one of them is used). The capture and registration processes are more convenient compared to other multispectral imaging schemes [5]. This scheme has highly accurate colorimetric reproduction [6]. However, it does not produce sufficient spectral accuracy. For example, the spectral reproduction is not accurate enough for pigment mapping [7]. A two-in-one multispectral-stereo system was proposed by [8], using two RGB camera with a pair of filters in front of them to produce six-channel imaging. However, stereo matching algorithms are needed to process the images after capture.

For wide band capture, a good compromise between spectral accuracy and simplicity can be achieved. This paper will demonstrate the filter selection methods for a wide band capturing system. A lot of studies has been done for filter selection for multispectral imaging systems, such as [9] and [10] etc. The methods proposed in this paper based on spectral sensitivity modeling, also considered filters' noise propagation properties.

Modeling and Optimizing Spectral Sensitivity Considering Noise Propagation

Spectral Sensitivity Modeling

The spectral sensitivity model should meet physical restrictions. The transmittance should be larger than zero and not exceed unity. The shape of the spectral transmittance should be smooth. A model in [11] is applied here. The spectral sensitivity curves are defined with Gaussian functions:

$$S_i(\lambda) = e^{\left[-\frac{(\lambda-\lambda_i)^2}{w_i^2}\right]} \tag{1}$$

where λ is wavelength, λ_i is peak wavelength, and w_i is half bandwidth. $i = R, G, B$. Example plots are shown in Fig. 1.

Color Space Transformation Modeling

The color transformation matrix M is defined as

$$M = \begin{pmatrix} m_1 & m_2 & m_3 \\ m_4 & m_5 & m_6 \\ m_7 & m_8 & m_9 \end{pmatrix} \tag{2}$$

where

$$\begin{pmatrix} X/X_n \\ Y/Y_n \\ Z/Z_n \end{pmatrix} = M \times \begin{pmatrix} C_1/C_{1,n} \\ C_2/C_{2,n} \\ C_3/C_{3,n} \end{pmatrix} \tag{3}$$

and

$$m_1 + m_2 + m_3 = m_4 + m_5 + m_6 = m_7 + m_8 + m_9 = 1 \tag{4}$$

m_1 to m_9 are the coefficients in the color transformation matrix. X_n, Y_n,Z_n are the tristimulus value of white. When the input is

neutral, the output is neutral. The corresponding constraints are shown in Eq. 4, which enable the neutral camera signal to be mapped to the colorimetric neutral output. The C_i is the camera signal:

$$C_i = \int_{\lambda 1}^{\lambda 2} S_{i,\lambda} \times L_\lambda \times R_\lambda \tag{5}$$

where $S_{i,\lambda}$ corresponds to the sensor spectral sensitivity, L_λ is the spectral radiance of the light source, and R_λ is the spectral reflectance of a sample.

Optimization of Seven Channel Bandpass Filter Set Modeling

An optimal set of seven channel bandpass filter for D50 illumination and a FLI PL50100 monochrome camera which will be used to build the spectral camera was calculated. The ColorChecker SG (CCSG) was used as the training data set to optimize the color transformation matrix. The Artist Paint Target (APT) was used as the validation data set.

A matrix including the peak wavelengths λ = 400, 450, 500, 550, 600, 650, 700nm, the half bandwidths w = 60nm for all of them was used as the starting value to non-linearly minimize Q (fminunc in MATLAB, trust-region algorithm) which is defined in Eq. 6. Starting values with the same peak wavelengths and different half bandwidths were tested for the optimization and the same result was obtained.

$$Q = \alpha \times (100 * \overline{RMS}) + \beta \times \overline{\Delta E_{00}} + (1 - \alpha - \beta) \times \overline{N} \tag{6}$$

where RMS is the root-mean-square error of the spectral reflectance difference between the measured data and predicted data, and it is scaled by 100 to agree with the order of magnitude of ΔE_{00} and N. N is the propagated noise, not including photon shot noise.

Using the model in [11], the propagated color noise N for neutral patches from the color transformation matrix is calculated using the following equation:

$$N = (\Delta L^{*2} + \Delta a^{*2} + \Delta b^{*2})^{1/2} \tag{7}$$

and ΔL^* , Δa^* and Δb^* are calculated in eq. 8 to eq. 10, which are the sum of the square of different rows of color transformation matrix coefficients (or the subtraction results of them) with different weightings.

$$(\triangle L^*)^2 \simeq \left(\frac{116A}{3}\right)^2 (m_{21}, m_{22}, m_{23})^2 \tag{8}$$

$$(\triangle a^*)^2 \simeq \left(\frac{500A}{3}\right)^2 \{(m_{11}, m_{12}, m_{13}) - (m_{21}, m_{22}, m_{23})\}^2 \tag{9}$$

$$(\triangle b^*)^2 \simeq \left(\frac{200A}{3}\right)^2 \{(m_{21}, m_{22}, m_{23}) - (m_{31}, m_{32}, m_{33})\}^2 \tag{10}$$

α and β are the weighting factors of the RMS and the ΔE_{00}. Different weightings were tested (Table 1): optimized for just RMS ($\alpha = 1; \beta = 0$), just ΔE_{00} ($\alpha = 0; \beta = 1$), just N ($\alpha = 0; \beta = 0$), $RMS + \Delta E_{00}$ ($\alpha = 0.5; \beta = 0.5$), $RMS + N$ ($\alpha = 0.5; \beta = 0$), $\Delta E_{00} + N$ ($\alpha = 0; \beta = 0.5$), and equal weighting ($\alpha = 0.3; \beta = 0.3$). An equal weighting ($\alpha = \beta = 0.3$) was chosen for the optimization. In different applications, different weighting factors could be used and would lead to different results. For example, the weighting of the RMS could be raised if the goal is to achieve high spectral reproduction accuracy. The result is shown in Fig. 2. The corresponding data are shown in Table 2.

Table 1: The ΔE_{00},N and RMS for theoretical Gaussian filters with different optimization parameters.

α	β	RMS	ΔE_{00}	N
0.3	0.3	0.014	0.11	1.05
1	0	0.013	0.59	509.76
0	1	0.018	0.02	3.75
0	0	0.022	1.07	0.82
0.5	0.5	0.014	0.07	42.42
0.5	0	0.014	1.31	0.88
0	0.5	0.034	0.04	0.84

The approximated color matching functions (Fig. 3) are the product of the seven filter spectral sensitivities and their corresponding optimal color transformation matrix. The color matching functions were well approximated by the seven filter sensitivities. μ-factor [12] is a colorimetric performance metric with respect to the mean-square error between a set of color matching functions and its estimation, which is expressed as:

$$\mu = Trace(S' A^{\dagger} \times A' \times S^{\dagger})/3 \tag{11}$$

where S is the product of estimated color matching function and the viewing illuminant radiance, A is the product of standard color matching function and imaging illuminant radiance [12]. For the optimized seven filter set, $\mu = 0.983$, which represents a highly accurate color matching function estimation.

Table 2: Optimal seven filter spectral sensitivity for $\alpha = 0.3$, $\beta = 0.3$. (unit:nm)

peak	389	449	515	551	596	629	725
bandwidth	56	62	68	62	52	68	74

Schott Sandwich Filter Selection

Schott filters can be glued together to have bandpass shapes, which can be used to build the spectral camera. The glued Schott filters will be called "sandwich filter" as an abbreviation in the following discussions. Two methods were tested to find the optimal set of sandwich filters. For the first method, sandwich filters which have the most similar spectral transmittance as the theoretical Gaussian filters in the previous section were selected. For the second method, sandwich filters whose peak wavelength were equally spaced across the spectrum of interest were tested as candidate filters and selected according to their spectral and colorimetric reproduction accuracy.

The spectral transmittance $T_{combination,\lambda}$ of the combination of two candidate filters ($T_{1,\lambda}, T_{2,\lambda}$) was calculated using the Eq.12. This equation represents the signal after flat-fielding, as well as changing exposure time or energy to maximize signal.

The spectral transmittance just refers to internal spectral transmittance, ignoring surface reflection.

$$T_{combination,\lambda} = T_{1,\lambda} \cdot T_{2,\lambda} / max(T_{1,\lambda} \cdot T_{2,\lambda}) \quad (12)$$

Method 1: Fitting Gaussians

The selection was based on the available Schott filter database from SCHOTT and Andover Corporation [13]. Since the final spectral sensitivities have Gaussian shapes, the width and peak wavelength position of the candidate filters should be located within a limited continuous solid. Therefore, the Schott filters were pre-selected first. Filters whose spectral transmittance shape are smooth and with single or double peaks locating between 400nm-700nm were pre-selected. The number of candidate filters were reduced from 64 to 52 for the Schott database, and 41 to 33 for the Andover database.

The RMS between each sandwich filter and each theoretical Gaussian filter was calculated. The optimal sandwich filters should have similar shapes as the theoretical Gaussian filters, and the optical throughputs should not be low. Therefore, the filter combinations whose RMS between the $T_{combination}$ and the theoretical Gaussian filters is the smallest and peak spectral transmittance is larger than 0.3 (or any other reasonable minimum peak to meet the application requirements), were selected as candidate filters. Filters which cause high near infrared throughputs were replaced manually since the monochrome camera is sensitive in the near infrared region.

The final selected filters are shown in Table 3 and Fig. 4. The throughput of the fourth channel (the channel which is closet to V_λ) is the highest, indicating bright luminance channel. The estimated spectral and colorimetric reproduction are shown in Fig. 5.

Table 3: The final selected filters.

# sandwich filter	Filter 1	Filter 2
1#	BG25	BG25
2#	BG12	GG420
3#	BG23	GG495
4#	OG530	S8612
5#	BG40	OG570
6#	BG38	OG590
7#	KG5	RG665

Table 4: The ΔE_{00},N and RMS for theoretical Gaussian filters and selected sandwich filters.

	RMS	ΔE_{00}	N
Theoretical Gaussian filters	0.014	0.11	1.05
Sandwich filters	0.019	0.28	1.08

Method 2: Subsets Selection Method

Instead of trying to calculate corresponding metric values for all possible combinations (4.3×10^{10}) of filters, a more efficient way is to divide the spectrum of interest (400nm-750nm) evenly and select the combinations of filters whose peak wavelength were located in the range of spectrum subsets manually. The candidate filter combinations were reduced to 1.8×10^6.

Seven-layer for-loops were built to calculate metric values for all possible combinations of the pre-selected filters. RMS, ΔE_{00} and noise were calculated using the technique and equations as is shown in the seven channel bandpass filter set modeling. The cost function Q is defined as:

$$Q = 40 \times \overline{RMS} + 3 \times \overline{\Delta E_{00}} + 1 \times \overline{N} \quad (13)$$

The scale factors were decided based on preliminary results with aim of incorporating filter combinations which have low noise for the next-step selection.

Filter combinations were sorted in an ascending order for Q and top 1000 were selected for further analysis. Histograms of ΔE_{00}, noise and RMS are shown in Fig. 6.

K-means classification method was used to classify the top 1000 combinations. The results are shown in Fig. 7. The sandwich filters marked with blue circles have lowest noise, and their ΔE_{00} are 0.7-0.9, which are high as is shown in the first plot in Fig. 6. There is a trade-off between noise and ΔE_{00}, which is in line with [11]. Comparing the results of fitting Gaussian method (N 1.08, ΔE_{00} 0.28, RMS 0.019), for the top 1000 combinations whose noise are less than 1.6, ΔE_{00} are larger than 0.7. Therefore, the filters selected using the fitting Gaussian method were selected to build the multispectral camera.

Single Schott Filter Selection

This section will describe single Schott filters selection for the same monochrome camera. Single Schott filters have high optical throughput, giving high signal-to-noise ratio. Moreover, the transmittance does not shift with incident angles compared to that of interference filters. Using off-the-shelf single Schott filters can avoid gluing procedure. Also, it is cost-effective.

A UV/IR cut filter was included in the filter selection process since preliminary selected filters have high near infrared optical throughput. Seven-layer for-loops were built to calculate metric values for all possible combinations of filters manufactured by Schott. RMS and noise were calculated using the technique and equations as is shown in the seven channel bandpass filter set modeling. The cost function Q is defined as:

$$Q = 400 \times \overline{RMS} + \overline{N} \quad (14)$$

The scale factors were decided based on preliminary results with aim of incorporating filter combinations which have low noise for next-step selection.

Filter combinations were sorted in an ascending order for Q and top 300 were selected for further analysis. Histograms of ΔE_{00}, noise and RMS are shown in Fig.8.

K-means classification method was used to classify the top 300 combinations. The results are shown in Fig. 9. The green group was selected since it has lowest ΔE_{00} and noise, although it has medium RMS (0.022-0.024), which is acceptable.

Table 5: Results of selected filters in Fig.10.

RMS	ΔE_{00}	N
0.023	0.25	4.21

Nonlinear optimization for ΔE_{00} was taken for the green group. The filter set whose ΔE_{00} was the smallest was selected. The selected filters are shown in Fig. 10 and the results are shown in Table 5. Spectral reproduction results is shown in the first and second plot in Fig. 11. The long wavelength part has more errors because of the inclusion of the UV/IR cut filter. Tone reproduction results is shown in the third plot in Fig.11. The errors are very small. Color reproduction results is shown in the fourth plot in Fig.11. The errors are very small.

Conclusions

The spectral sensitivities of seven channel bandpass filters were modeled by Gaussian functions and optimized with the considerations of RMS, the color accuracy and the propagated noise. Off-the-shelf Schott sandwich filters were used to realize the theoretical optimal Gaussian filters. Two methods were used to select the sandwich filters considering spectral and colorimetric reproduction accuracy, noise and throughput for visible and UV/IR range. Compared to the traditional subsets selection method, the fitting Gaussians method was much more efficient and generated better results. The sandwich Schott filters can yield accurate spectral and colorimetric reproduction and low noise in terms of small RMS, ΔE_{00} and N.

For single Schott filters selection, UV/IR cut filter was included because of the sensor's infrared sensitivity. The spectral and colorimetric reproduction of the selected filter set is accurate. However, although the signal-to-noise ratio is high, the propagated noise is still high compared to the sandwich filters because of the large overlaps between the filters. Therefore, the glued Schott filters are more preferred.

The outcome filter set as well as the spectral sensitivity modeling and optimization technique can provide insights for filter selection and signal encoding in multi-spectral camera design.

References

[1] Brauers, Johannes, Nils Schulte, and Til Aach. "Multispectral filterwheel cameras: Geometric distortion model and compensation algorithms." Image Processing, IEEE Transactions on 17, no. 12 (2008): 2368-2380.

[2] Novati, Gianluca, Paolo Pellegri, and Raimondo Schettini. "An affordable multispectral imaging system for the digital museum." International Journal on Digital Libraries 5, no. 3 (2005): 167-178.

[3] Fischer, Christian, and Ioanna Kakoulli. "Multispectral and hyperspectral imaging technologies in conservation: current research and potential applications." Studies in Conservation 51, no. sup1 (2006): 3-16.

[4] Bianco, Simone, Alessandro Colombo, Francesca Gasparini, Raimondo Schettini, and Silvia Zuffi. "Applications of spectral imaging and reproduction to cultural heritage." Digital Imaging for Cultural Heritage Preservation (2011): 183-209.

[5] Taplin, Lawrence, and Roy Berns. "Practical spectral capture systems for museum imaging." Association Internationale de la Couleur (AIC)-International Color Association (2005).

[6] Berns, Roy, Lawrence Taplin, and Mahdi Nezamabadi. "Modifications of a sinarback 54 digital camera for spectral and high-accuracy colorimetric imaging: simulations and experiments." (2004).

[7] Abed, Farhad Moghareh. "Pigment Identification of Paintings Based on Kubelka-Munk Theory and Spectral Images." (2014).

[8] Shrestha, Raju, Jon Yngve Hardeberg, and Alamin Mansouri. "One-shot multispectral color imaging with a stereo camera." Proc. SPIE. Vol. 7876. 2011.

[9] Hardeberg, Jon Y. "Filter selection for multispectral color image acquisition." Journal of Imaging Science and Technology 48.2 (2004): 105-110.

[10] Day, David C. "Filter Selection for Spectral Estimation Using a Trichrmatic Camera." (2003).

[11] Kuniba, Hideyasu, and Roy S. Berns. "Spectral sensitivity optimization of color image sensors considering photon shot noise." Journal of Electronic Imaging 18, no. 2 (2009): 023002-023002.

[12] Vora, Poorvi L., and H. Joel Trussell. "Measure of goodness of a set of color-scanning filters." JOSA A 10, no. 7 (1993): 1499-1508.

[13] https://www.andovercorp.com/products/colored-glass/general-specifications/

List of Figures

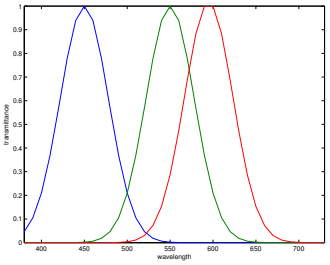

Figure 1: Spectral sensitivity curves with peak wavelength of 595nm, 550nm, 450nm and half bandwidth of 40nm for all.

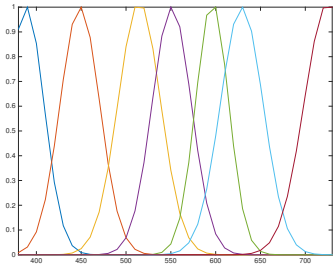

Figure 2: Optimal seven bandpass filters.

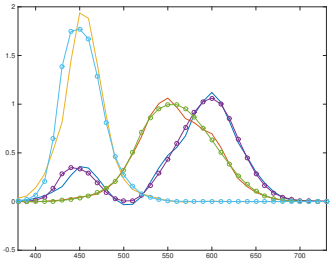

Figure 3: Lines: estimated color matching functions using the optimal seven bandpass filters. Circle lines: color matching functions.

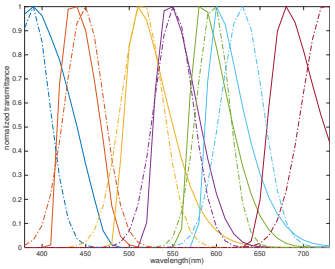

(a) Normalized spectral transmittance. Dash lines: theoretical Gaussian filters. Solid lines: selected sandwich filters.

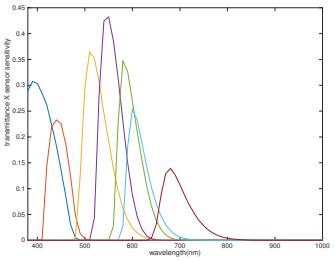

(b) Spectral sensitivity of the whole system including the FLI sensor and filters.

Figure 4: Final selected sandwich filters using fitting Gaussians method.

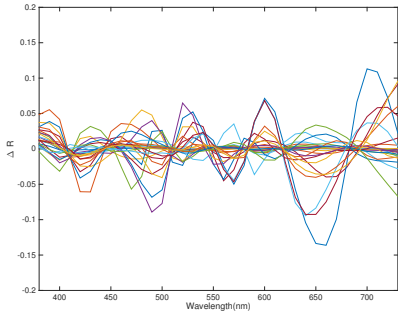

(a) Spectral reflectance difference between estimated and reference data for APT.

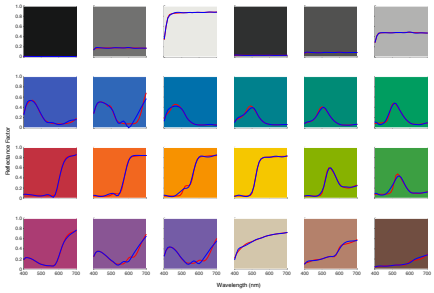

(b) Spectral reflectance difference between estimated and reference data for each patch of APT.

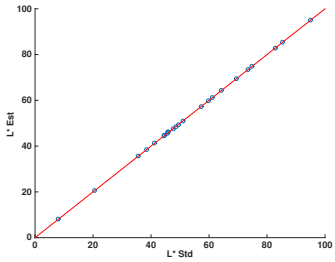

(c) Lightness difference between estimated and reference data for APT.

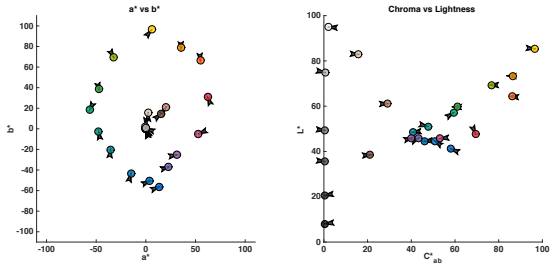

(d) a^*b^* and $L^*C^*_{ab}$ difference between estimated and reference data for APT.

Figure 5: The difference between the estimated and reference spectral and colorimetric reproduction for fitting Gaussians method.

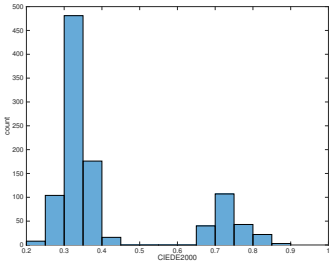

(a) ΔE_{00} histogram.

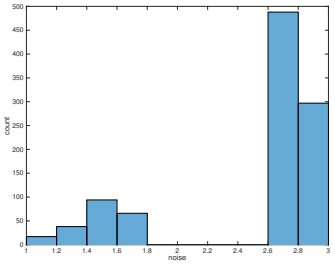

(b) Propagated noise histogram.

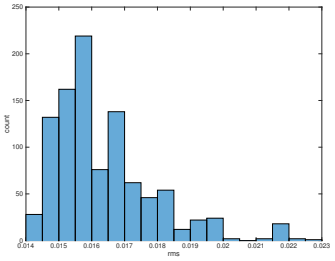

(c) RMS histogram.

Figure 6: Histograms of ΔE_{00}, noise and RMS for subsets selection method.

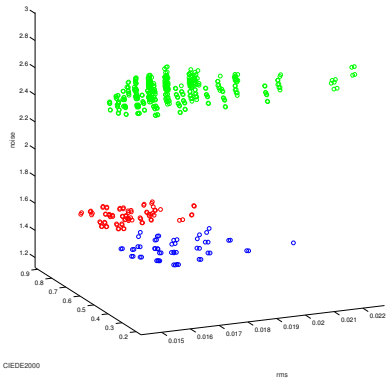

(a)

Figure 7: K-means classification results for subsets selection method.

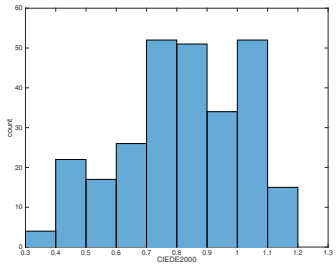

(a) ΔE_{00} histogram.

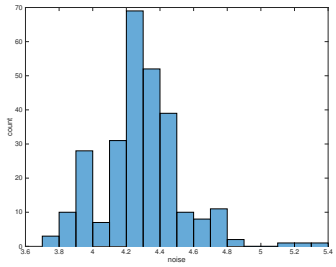

(b) Propagated noise histogram.

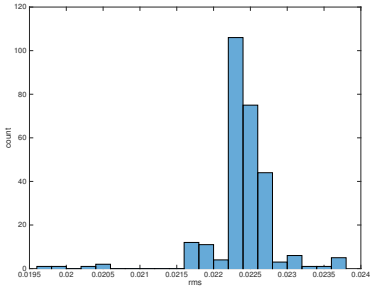

(c) RMS histogram.

Figure 8: Histograms of ΔE_{00}, noise and RMS for single Schott filter selection.

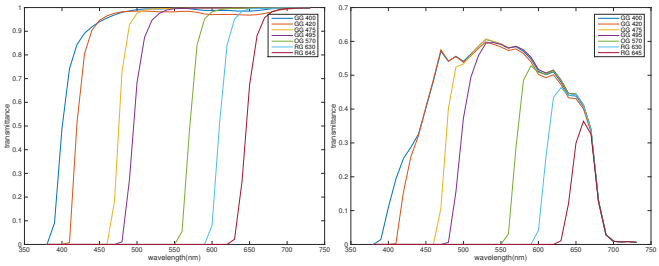

(a) Selected filter transmittance. (b) System spectral sensitivity.

Figure 10: Selected filter transmittance and system spectral sensitivity for single Schott filter selection.

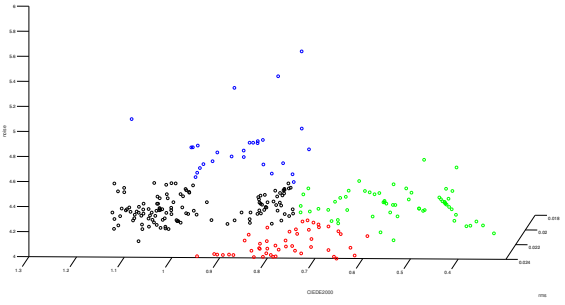

(a)

Figure 9: K-means classification results for single Schott filter selection.

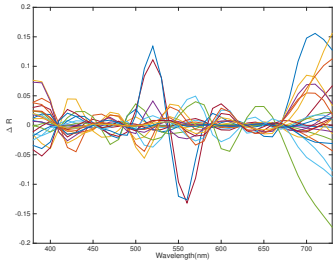

(a) The difference between estimated and reference spectral reflectance for APT.

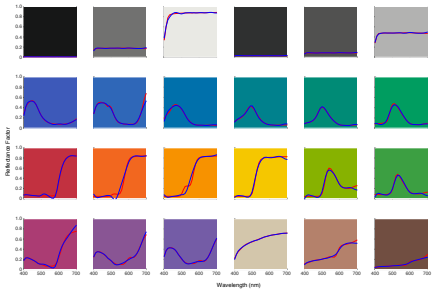

(b) Estimated and reference spectral reflectance for APT.

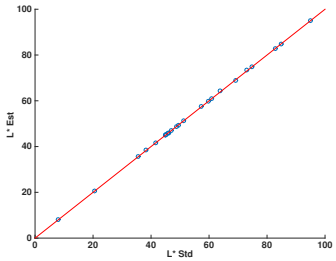

(c) Lightness difference between estimated and reference data for APT.

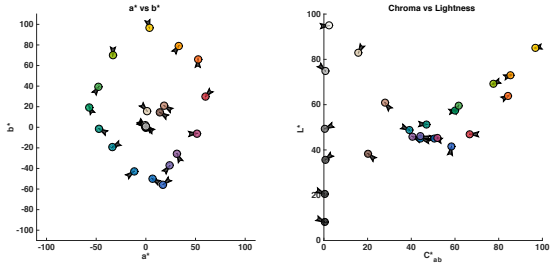

(d) a^*b^* and $L^*C^*_{ab}$ difference between estimated and reference data for APT.

Figure 11: The difference between the estimated and reference spectral and colorimetric reproduction for single Schott filter selection.